Modified Connective Assembly Model for Error Propagation Analysis of High-Precision Assembly of Mechanical Components

Muhammad Arif [1,*], Tanweer Hussain [1], Nayyar Hussain Mirjat [2], and Asif Ali Shaikh [3]

[1] Department of Mechanical Engineering, Mehran University of Engineering and Technology, Jamshoro, Pakistan
[2] Department of Electrical Engineering, Mehran University of Engineering and Technology, Jamshoro, Pakistan
[3] Department of Basic Sciences and Related Studies, Mehran University of Engineering and Technology, Jamshoro, Pakistan
Email: m.arif@buetk.edu.pk (M.A.); tanweer.hussain@faculty.muet.edu.pk (T.H.); nayyar.hussain@faculty.muet.edu.pk (N.H.M.); asif.shaikh@faculty.muet.edu.pk (A.A.S.)
*Corresponding author

***Abstract*—High-precision mechanical assemblies require accurate error propagation models to predict error accumulation in the final assembly and ensure optimal performance and reliability. Conventional linear models exhibit limited accuracy in predicting geometric errors. To address these limitations, this study proposes a modified connective assembly model based on second-order nonlinear error propagation using homogeneous transformation matrices. The model is implemented in Python and validated against existing linear and fully nonlinear assembly models to evaluate predictive accuracy and computational efficiency. At an angular orientation error of 1.0°, the linear model exhibits Z-direction errors of 0.40 mm, 0.60 mm, and 0.80 mm for 4, 6, and 8 component assemblies, respectively, whereas the fully nonlinear model predicts 0.10 mm, −0.57 mm, and −2.18 mm. The developed model reduces these discrepancies to 0.23 mm, −0.25 mm, and −1.59 mm, achieving improved predictive accuracy of 56.67%, 72.65%, and 80.20%, respectively, over the linear model. Similarly, under a geometric run-out tolerance of 1.0 mm, the linear model predicts an error of −1.60 mm, −2.40 mm, and −3.20 mm, compared to −1.70 mm, −2.79 mm, and −4.18 mm for the fully nonlinear model in the Z-direction. The proposed model narrows these gaps to −1.66 mm, −2.68 mm, and −3.99 mm, delivering predictive accuracy of 60.00%, 71.79%, and 80.61%, respectively. Moreover, Monte Carlo simulation results on 4-component assembly confirm that the proposed model replicates the statistical characteristics of the fully nonlinear model while reducing execution time from 9.34 s to 4.82 s, achieving a 48.39% reduction in execution time.**

***Keywords*—high precision components, mechanical assemblies, variation propagations, modified connective assembly model**

I. Introduction

The reliability, longevity, and performance of high-precision mechanical assemblies mainly depend on the dimensional and geometric accuracy of their individual components, and the style in which these components are assembled [1]. However, due to manufacturing imperfections, the components are often produced with geometric errors. During the assembly process, these component-level geometric errors propagate through the mating surfaces and accumulate, ultimately causing the final assembly to deviate from its intended nominal geometry [2]. These geometric errors affect not only the assembly's functionality and dimensional accuracy but also its mechanical behavior, long-term stability, and overall performance.

In order to address these aforementioned challenges, a substantial body of research has focused on modeling geometric errors and their propagation using connective assembly models to improve prediction accuracy in assembled components. For instance, a precision prediction method developed for aero-engine rotors by incorporating surface morphology and non-uniform contact deformation, which achieved a 10.6% improvement in accuracy and a 60.2% reduction in coaxiality errors using a genetic algorithm-based phase optimization approach [3]. The stage-by-stage propagation of mass eccentric deviations in multistage rotors was analyzed through the development of a constrained nonlinear programming model, which employed a genetic algorithm to minimize initial unbalance in aero-engine multistage rotors [4]. Similarly, the orientation of individual rotors was optimized in order to minimize axial deviations in multistage assemblies, and this approach was further extended to integrate Monte Carlo simulations to more effectively control assembly eccentricity [5, 6]. Similar strategies have also been applied to 2D axisymmetric rotors by minimizing radial Root-Mean-Square (RMS) errors at rotor interfaces [7]. In order to improve the assembly accuracy, location and orientation tolerances are considered to reduce cumulative eccentric deviations by nearly 50% compared to the direct

Manuscript received July 14, 2025; revised August 25, 2025; accepted October 15, 2025; published January 9, 2026.

build methods [8]. This strategy was further improved through an adjustment technique that incorporated eccentric and tilt rotor stages and achieved 71% and 57% maximum and average error reduction respectively, for multistage rotor assemblies [9].

In order to mitigate such type of effects, predictive models have incorporated decoupling algorithms that integrate manufacturing variation data with intermediate measurements [10]. Coaxiality measurement methods using common datum axes have also been proposed to improve accuracy and reduce deviations in aero-engine rotor assemblies [11]. In parallel to this, deviation propagation models based on Jacobian-Torsor theory have been introduced to provide general formulations for n-stage rotor assemblies that incorporate deviation propagation functions and optimization objectives [12, 13]. Further contributions in this area include repair decision-making frameworks [14], datum error elimination strategies [15], and optimization approaches that integrate tensor coordinate transformations with multi-objective algorithms [16]. Multi-degree-of-freedom Numerical Control (NC) platforms, combined with Monte Carlo simulations, have also been employed to evaluate and improve docking accuracy in precision assemblies [17, 18].

In addition to these analytical approaches, recent studies have explored probabilistic tolerance analysis methods [19], where deviation propagation is modeled statistically to account for manufacturing uncertainty distributions. Meanwhile, deep learning-based prediction methods [20] have emerged, using data-driven surrogates to model nonlinear assembly behavior and provide rapid predictions. Similarly, digital twin modeling [21] has gained attention as a way to integrate real measurement data and simulations, enabling adaptive control of variation during assembly. While these approaches are powerful, but often rely on extensive datasets, high computational resources, or continuous data integration, which may limit their applicability in early design-phase analysis.

Early formulations of assembly variation propagation include the linear model, which offers computational simplicity but may compromise accuracy, and the fully nonlinear model, which achieves high fidelity at the cost of significant computational demand [22]. In order to address these limitations, the proposed study introduces a modified connective assembly model that incorporates second-order nonlinear error propagation using Homogeneous Transformation Matrices (HTMs). Unlike the fully nonlinear model, which retains all orders of nonlinear terms and trigonometric expansions, the proposed model retains only second-order nonlinear terms in the matrix multiplication.

This formulation enables it to maintain higher predictive accuracy than the linear model, while reducing execution time compared to the fully nonlinear model, thereby positioning it as a novel intermediate model that effectively balances predictive accuracy and computational efficiency. In order to underscore the novelty of this study, Table I summarizes the comparative features of the proposed model against the fully nonlinear, linear, and Jacobian-Torsor models, emphasizing the key differences among these approaches.

TABLE I. NOVELTY COMPARISON OF MODIFIED MODEL WITH THE EXISTING MODELS

Aspect	Fully Nonlinear Model	Modified Model	Linear Model	Jacobian-Torsor
Predictive Accuracy	Highest	High	Lowest	Moderate
Nonlinear terms	All orders retained	Up to 2nd order (closed form)	First-order only	Varies by expansion
Error Propagation	Full nonlinear expansion	Retains 2nd order nonlinear effects	Simple	Recomputed using Jacobians
Matrix operations	Fully nonlinear matrices	2nd order nonlinear terms	Linearized	Jacobian only
Numerical stability	High across all ranges	Stable at small to moderate deviations	Unstable in nonlinear regimes	Sensitive
Execution Time	Slowest	Moderate	Fastest	Moderate-High
Interpretability	Complex	Moderate	Simple	Moderate
Memory requirements	Highest	Low to moderate	Minimal	Higher
Implementation effort	High	Moderate	Low	Moderate-High

This comparative analysis highlights the balanced performance of the proposed model, demonstrating its potential to improve predictive accuracy without the computational and implementation burdens of fully nonlinear approaches.

All computations in this study were performed using the python programming language within a Jupyter Notebook platform. Core computational tasks were performed using the NumPy library for efficient matrix operations and numerical analysis, while Matplotlib was employed for visualizing results. All simulations and analyses were carried out on a Dell Inspiron 5502 laptop equipped with an 11th Gen Intel(R) Core(TM) i7-1165G7 CPU @ 2.80 GHz, 8 GB of RAM, and a 64-bit Windows 11 operating system.

The structure of the paper is organized as follows: Section II describes the methodology used to develop the modified connective assembly model. Section III provides a detailed analysis of the developed model, while Section IV validates the effectiveness of the proposed model. Section V discusses the key findings, and Section VI concludes the paper.

II. RESEARCH METHODOLOGY

The research methodology adopted for the development of the modified connective assembly model, as shown in

Fig. 1, is structured to define component tolerances, represent manufacturing variations through nominal and differential transforms, and evaluate the propagation and accumulation of these variations within the assembly process.

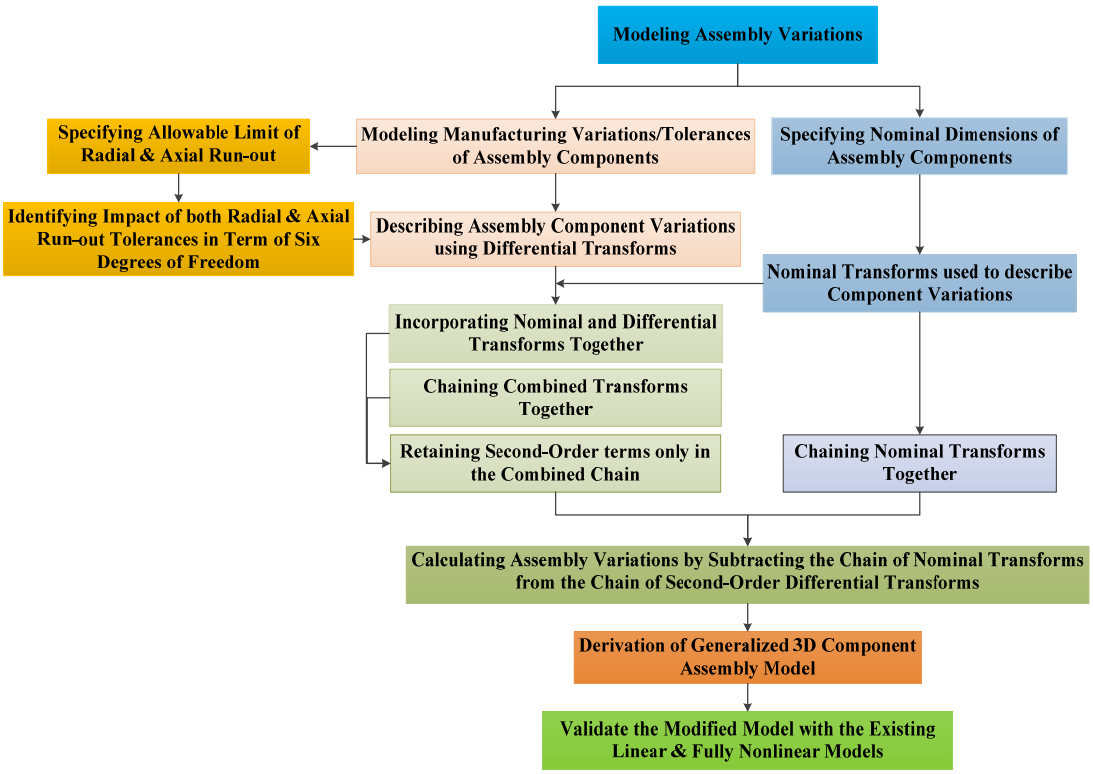

Fig. 1. Research methodology flow chart for developing the modified connective assembly model.

A. *Development of a Modified Connective Assembly Model*

Connective assembly models [23] are employed to quantify the propagation of component-level variations throughout the assembly process. These models use matrix transformations to describe the spatial relationships between coordinate frames attached to the mating features of adjacent components. For Three-Dimensional (3D) components, the geometric relationship between any two coordinate frames is illustrated in Fig. 2.

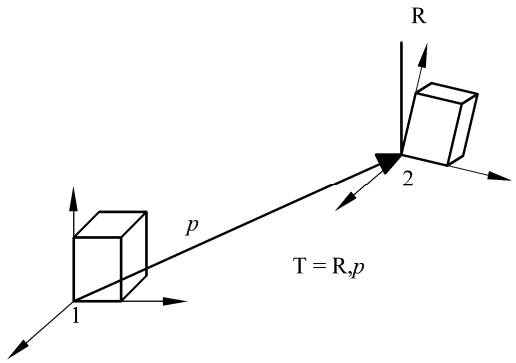

Fig. 2. Geometric relationship between two coordinate frames [23].

As shown in Fig. 2, the geometric relationship between coordinate frames 1 and 2 is represented by a matrix transform T. This matrix transform captures both rotation and translation operations acting on a coordinate frame aligned with a reference frame [23] and is given in Eq. (1).

$$T = \begin{bmatrix} R & p \\ 0^T & 1 \end{bmatrix} \tag{1}$$

Here, R is a 3×3 rotation matrix representing the orientation of frame 2 relative to frame 1, and p is a 3×1 position vector indicating the location of frame 2 relative to frame 1. The superscript T denotes the matrix transpose.

In a three-component assembly, as shown in Fig. 3(a), the model assumes that the components are assembled sequentially through their mating features [23]. Transformation matrices are used to define the position and orientation of each component relative to these mating features under nominal conditions. For the assembled configuration shown in Fig. 3(b), the transformation matrix representing the cumulative position and orientations from the base of component 1 to the top of component 3 is denoted as $T^N_{0\to3}$. This cumulative transformation is obtained by multiplying the individual nominal transformation matrices along the assembly sequence, is given in Eq. (2).

$$T^N_{0\to3} = T^N_{0\to1} \times T^N_{1\to2} \times T^N_{2\to3} \tag{2}$$

Here, $T^N_{0\to1}$ represents the transformation matrix that relates the position and orientation of the coordinate frame from feature 0 to feature 1 on component 1. Similarly,

$T_{1\to2}^{N}$ defines the transformation within component 2, from feature 1 to feature 2. Finally, $T_{2\to3}^{N}$ describes the transformation from the mating feature 2 to the top of component 3. All these transformation matrices follow the general form as in Eq. (1). Superscript *N* reflects nominal geometry between the mating features.

Under the axisymmetric property of components, the rotation matrix R is the identity matrix in Eq. (1), representing the relative orientation between the frames, and the position vector p is a zero vector except in the Z-direction. The nominal individual transformation matrices for the assembly of three components can be written as in Eqs. (3)–(6).

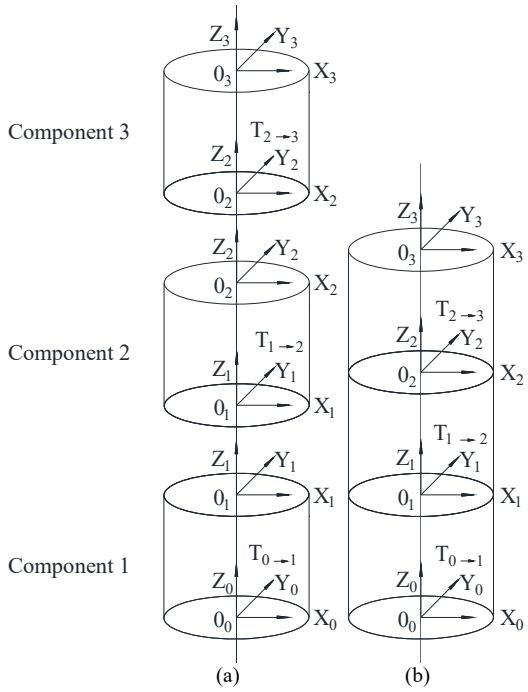

Fig. 3. Example of a three-component assembly: (a) before assembly, (b) after assembly.

$$T_{0\to1}^{N}=\begin{bmatrix} I & p_1^N \\ 0^T & 1 \end{bmatrix} \tag{3}$$

$$T_{1\to2}^{N}=\begin{bmatrix} I & p_2^N \\ 0^T & 1 \end{bmatrix} \tag{4}$$

$$T_{2\to3}^{N}=\begin{bmatrix} I & p_3^N \\ 0^T & 1 \end{bmatrix} \tag{5}$$

$$P_i^N=\begin{bmatrix} 0 \\ 0 \\ Z_i \end{bmatrix} \tag{6}$$

Z_i in Eq. (6) is the height of the i^{th} component. Substituting Eqs. (3)–(5) into Eq. (2) yields Eq. (7). In Eq. (8), $T_{0\to n}^{N}$ is the transformation matrix representing the assembly of n components, which relates the location and orientation of the coordinate frame at the top of component n to the coordinate frame at the base of component 1.

$$T_{0\to3}^{N}=\begin{bmatrix} I & p_1^N+p_2^N+p_3^N \\ 0^T & 1 \end{bmatrix} \tag{7}$$

$$T_{0\to n}^{N}=\begin{bmatrix} I & \sum_i^n p_i^N \\ 0^T & 1 \end{bmatrix} \tag{8}$$

In real practice, components often exhibit small misalignments or dimensional deviations from their nominal geometry. These imperfections introduce position and orientation errors at mating features during assembly. To incorporate these deviations into the assembly model, a differential matrix transform DT_i is introduced for each component. This matrix considers both rotational and translational errors and follows the same structure as the transformation matrix defined in Eq. (1) as written in Eq. (9).

$$DT_i=\begin{bmatrix} dR_i & dp_i \\ 0^T & 1 \end{bmatrix}, i=1,2,3 \tag{9}$$

Here, dp_i is the translation vector representing the deviation of the mating feature on component i from its nominal position, with small displacements along the x-, y-, and z-axes, as expressed in Eq. (10).

$$dP_i=\begin{bmatrix} dX_i \\ dY_i \\ dZ_i \end{bmatrix}, i=1,2,3 \tag{10}$$

The dR_i is the rotation matrix that considers small rotational errors due to manufacturing imperfections. These rotational deviations are modeled by three individual rotation matrices $dR_{\theta xi}$, $dR_{\theta yi}$, and $dR_{\theta zi}$, which represent rotations about the x, y, and z-axes, respectively [23]. The combined rotation error matrix dR_i is obtained by multiplying these individual rotation matrices together to achieve Eq. (11).

$$dR_i=\begin{bmatrix} Cd\theta_{yi}Cd\theta_{zi} & -Cd\theta_{yi}Sd\theta_{zi} & Sd\theta_{yi} \\ Sd\theta_{xi}Sd\theta_{yi}Cd\theta_{zi}+Cd\theta_{xi}Sd\theta_{zi} & Cd\theta_{xi}Cd\theta_{zi}-Sd\theta_{xi}Sd\theta_{yi}Sd\theta_{zi} & Sd\theta_{xi}Cd\theta_{yi} \\ Sd\theta_{xi}Sd\theta_{zi}-Cd\theta_{xi}Sd\theta_{yi}Cd\theta_{zi} & Cd\theta_{xi}Sd\theta_{yi}Sd\theta_{zi}+Sd\theta_{xi}Cd\theta_{zi} & Cd\theta_{xi}Cd\theta_{yi} \end{bmatrix} \tag{11}$$

where $Sd\theta$ and $Cd\theta$, denote $Sind\theta$ and $Cosd\theta$, respectively.

Applying small-angle approximations such that $Sd\theta=d\theta$ and $Cd\theta=1$ in Eq. (11), and assuming that the rotation angle errors are small, Eq. (11) can be approximated as Eqs. (12) and (13). Consequently, Eq. (9) becomes Eq. (14).

$$dR_i = I + \delta R_i \tag{12}$$

$$\delta R_i = \begin{bmatrix} 0 & -d\theta_{zi} & d\theta_{yi} \\ d\theta_{zi} & 0 & -d\theta_{xi} \\ -d\theta_{yi} & d\theta_{xi} & 0 \end{bmatrix} \tag{13}$$

$$DT_i = \begin{bmatrix} I + \delta R_i & dp_i \\ 0^T & 1 \end{bmatrix}, i=1,2,3 \tag{14}$$

For the three-component assembly, the total transformation from the base of component 1 (frame 0) to the top of component 3 (frame 3), considering the manufacturing variation, is given in Eq. (15). Substituting Eqs. (3)–(5) and (14) into Eq. (15) yields Eq. (16).

$$T_{0\to3} = T \times DT \tag{15}$$

$$T_{0\to3} = T_{0\to1}^{N} \times DT_1 \times T_{1\to2}^{N} \times DT_2 \times T_{2\to3}^{N} \times DT_3 \tag{16}$$

In Eq. (16), $T_{0\to1}^{N}$, $T_{1\to2}^{N}$ and $T_{2\to3}^{N}$ describe the nominal transformations assuming perfect manufacturing, while DT_1 , DT_2 and DT_3 represent the differential transformations considering the manufacturing variation in each component. The complete transformation incorporating both nominal and differential effects is shown in Eq. (17). After neglecting the third-order terms and keeping the terms up to second order only, the expression written as Eq. (18). The generalized summation form of Eq. (18) for the assembly of *n* components is written in Eq. (19).

$$T_{0\to3} = \begin{bmatrix} R_1R_2R_3 + R_1R_2\delta R_2R_3 + \\ R_1\delta R_1R_2R_3 + R_1\delta R_1R_2\delta R_2R_3 + \\ R_1R_2R_3\delta R_3 + R_1R_2\delta R_2R_3\delta R_3 + \\ R_1\delta R_1R_2R_3\delta R_3 + R_1\delta R_1R_2\delta R_2R_3\delta R_3 \\ 0^T \end{bmatrix} \begin{bmatrix} P_1 + R_1P_2 + R_1R_2P_3 + R_1dP_1 + R_1R_2dP_2 + \\ R_1\delta R_1P_2 + R_1\delta R_1R_2dP_2 + R_1R_2\delta R_2P_3 + \\ R_1\delta R_1R_2P_3 + R_1\delta R_1R_2\delta R_2P_3 + \\ R_1R_2R_3dP_3 + R_1R_2\delta R_2R_3dP_3 + \\ R_1\delta R_1R_2R_3dP_3 + R_1\delta R_1R_2\delta R_2R_3dP_3 \\ 1 \end{bmatrix} \tag{17}$$

$$T_{0\to3} = \begin{bmatrix} R_1R_2R_3 + R_1R_2\delta R_2R_3 + \\ R_1\delta R_1R_2R_3 + R_1\delta R_1R_2\delta R_2R_3 + \\ R_1R_2R_3\delta R_3 + R_1R_2\delta R_2R_3\delta R_3 + \\ R_1\delta R_1R_2R_3\delta R_3 \\ 0^T \end{bmatrix} \begin{bmatrix} P_1 + R_1P_2 + R_1R_2P_3 + R_1dP_1 + R_1R_2dP_2 + \\ R_1\delta R_1P_2 + R_1\delta R_1R_2dP_2 + R_1R_2\delta R_2P_3 + \\ R_1\delta R_1R_2P_3 + R_1\delta R_1R_2\delta R_2P_3 + R_1R_2R_3dP_3 + \\ R_1R_2\delta R_2R_3dP_3 + R_1\delta R_1R_2R_3dP_3 \\ 1 \end{bmatrix} \tag{18}$$

$$T_{0\to n} = \begin{bmatrix} \prod_{i=1}^{N} R_i \\ + \sum_{j=1}^{N} \left(\prod_{i=1}^{N} R_i \,.\, \delta R_j\right) \\ + \sum_{j=1}^{N} \left(\prod_{i=1}^{N} R_i \,.\, \delta R_i\, \delta R_j\right) \\ 0^T \end{bmatrix} \begin{bmatrix} \sum_{i=1}^{N} \left(\prod_{j=0}^{i-1} R_j\right) P_i + \sum_{i=1}^{N} \left[\prod_{j=1}^{i} (R_j) dP_i\right] \\ + \sum_{i=1}^{N-1} \left(\left(\prod_{j=1}^{i} R_j\right) \delta R_i \sum_{l=i+1}^{N} \left(\prod_{\substack{k=l-1 \\ k^1 1}}^{N-1} R_k\right) P_l\right) \\ + \sum_{i=1}^{N-1} \left(\left(\prod_{j=1}^{i+1} R_j\right) \delta R_i \delta R_j \sum_{l=i+1}^{N} \left(\prod_{\substack{k=l-1 \\ k^1 1}}^{N-1} R_k\right) P_i\right) \\ + \sum_{i=1}^{N-1} \left(\prod_{j=1}^{i} R_j\right) \delta R_i dP_j \\ 1 \end{bmatrix} \tag{19}$$

$$\begin{bmatrix} dp_i^X \\ dp_i^Y \\ dp_i^Z \end{bmatrix} = \begin{bmatrix} \sum_{i=1}^{N} \left[\prod_{j=1}^{i} (R_j) dP_i\right] + \sum_{i=1}^{N-1} \left(\left(\prod_{j=1}^{i} R_j\right) \delta R_i \sum_{l=i+1}^{N} \left(\prod_{\substack{k=l-1 \\ k^1 1}}^{N-1} R_k\right) P_l\right) \\ + \sum_{i=1}^{N-1} \left(\left(\prod_{j=1}^{i+1} R_j\right) \delta R_i \delta R_j \sum_{l=i+1}^{N} \left(\prod_{\substack{k=l-1 \\ k^1 1}}^{N-1} R_k\right) P_i\right) \\ + \sum_{i=1}^{N-1} \left(\prod_{j=1}^{i} R_j\right) \delta R_i dP_j \end{bmatrix} \tag{20}$$

The term, $T_{0\to n}$ in Eq. (19), represents the overall assembly transformation of n components, relating the position and orientation of the coordinate frame at the top of n^{th} component to the coordinate frame at the base of component 1, while considering second-order nonlinear effects induced by each component. Furthermore, the accumulated translation and rotational errors resulting from the assembly of N components are described in Eq. (20) which is used to calculate the translation errors dp_i^X, dp_i^Y and dp_i^Z after the assembly of i^{th} component.

B. *Specifying Allowable Limits for Radial and Axial Run-Outs*

Manufacturing processes introduce dimensional and geometric variations in components. These variations arise not only from process limitations but also from material properties, internal discontinues, and geometric properties of the component [24]. In order to consider these variations from the nominal, design engineers specify tolerances, which define allowable limits of variation for each component. Tolerances may be assigned to dimensions (e.g., size) or to features, thereby constraining allowable variations in shape, form, profile, or location of lines or surfaces.

C. *Identifying the Impact of Both Radial and Axial Runout Tolerances in Terms of Six Degrees of Freedom*

In order to evaluate the impact of component-level variations on assembly accuracy, these variations are described in terms of six Degrees of Freedom (DoF): three degrees of translational (dx, dy, dz) and three degrees of rotational $(d\theta_x, d\theta_y, d\theta_z)$ variations. For the purpose of modeling these variations, a 3D axisymmetric cylindrical component is analyzed under the combined effect of dimensional and geometric runout tolerances as depicted in Fig. 4(a). The radial runout (T_{rr}) controls the circular deviations of the component relative to the datum axis, while the axial runout tolerance (T_{ar}) controls surface deviations normal to the datum axis and the dimensional tolerance $(\pm T_s)$ specifies the allowable range for size variations.

Fig. 4(b) illustrates how the tolerance zone for axial runout is enclosed within the dimensional tolerance zone. The tolerance limit for radial runout (T_{rr}) is illustrated in Fig. 4(c), which shows the top view of the component. The radial runout results in a geometric shift of the component's actual circular profile from its ideal position, causing displacement in the x and y directions.

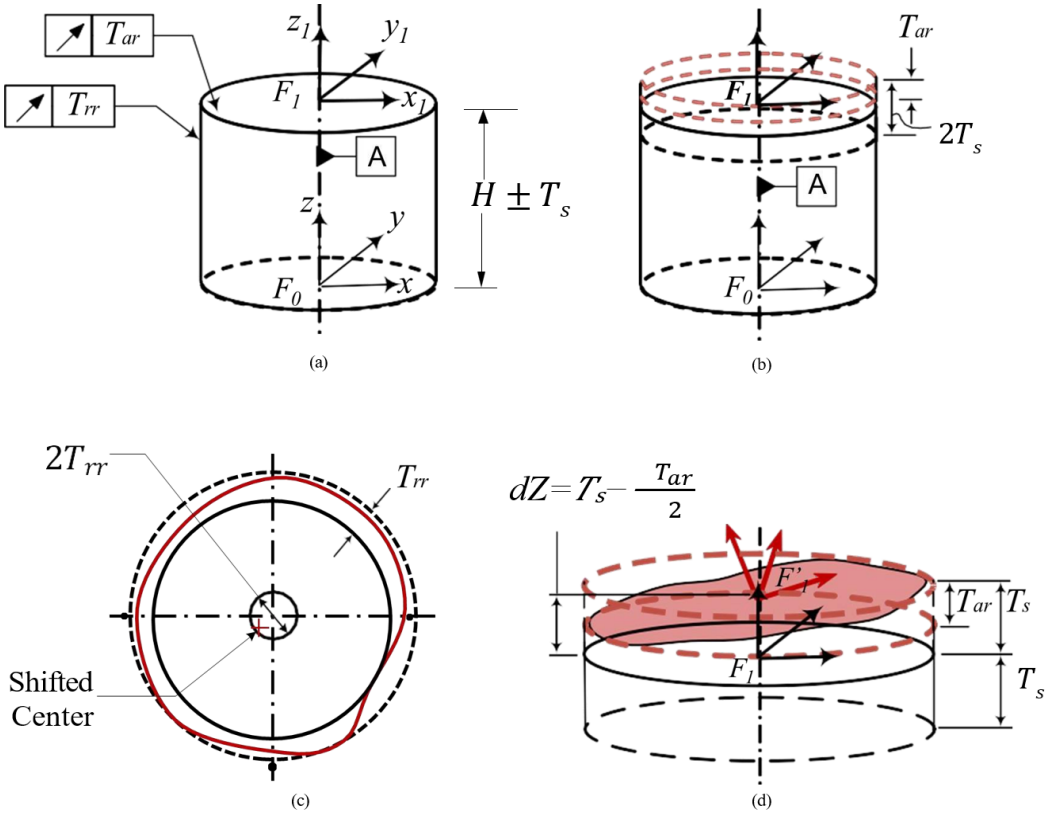

Fig. 4. Impact of radial and axial runouts on a 3D axi-symmetric cylindrical component: (a) tolerance applied; (b) axial run-out within size zone; (c) radial run-out causing eccentricity; (d) resulting position and tilt errors [22].

The constraint bounds for translation errors due to radial runout can be written in Eq. (21). The axial runout (T_{ar}) as depicted in

Fig. 4(d), introduces positional deviation along the z-axis as well as angular deviations about the x- and y-axes. Specifically, axial runout causes the top surface of the component to be tilted and shift from its nominal axis. When the angular deviation $(\delta\theta_x)$ occurs first, it consumes a portion of the allowable angular tolerance, thereby reducing the remaining range available for $(\delta\theta_y)$. Assuming the nominal diameter of the component is unaffected by dimensional errors, the

angular constraint bounds due to axial runout can be written as shown in Eqs. (22) and (23). Similarly, the positional deviations along the z-axis due to the combined effects of axial runout and dimensional tolerance can be written as shown in Eq. (24). Considering the combined effect of dimensional and runout tolerances, the complete variation vector across the six degrees of freedom for a 3D component can be written as shown in Eq. (25).

$$-T_{rr} \le dX \ge T_{rr} \text{ and } -T_{rr} \le dY \ge T_{rr} \quad (21)$$

$$-\tan^{-1}\frac{T_{ar}}{D} \le \delta\theta_x \le \tan^{-1}\frac{T_{ar}}{D} \quad (22)$$

$$-\left(\tan^{-1}\frac{T_{ar}}{D} - \delta\theta_x\right) \le \delta\theta_y \le \left(\tan^{-1}\frac{T_{ar}}{D} - \delta\theta_x\right) \quad (23)$$

$$-\left(T_s - \frac{T_{ar}}{2}\right) \le dZ \le \left(T_s - \frac{T_{ar}}{2}\right) \quad (24)$$

$$\left(dX, dY, dZ, d\theta_x, d\theta_y, d\theta_z\right)^T \quad (25)$$

where $d\theta_z = 0$.

III. Analysis of the Developed Model

This section presents an analysis of the assembly process involving the vertical stacking of four identical axisymmetric cylindrical components to form a straight structure, as illustrated in Fig. 5. The nominal dimensions and modeling assumptions for the analyzed assembly are illustrated in Fig. 6(a) and Table II. The components are assembled sequentially, starting with the first component placed concentrically on the geometric center of the assembly table. Each subsequent component is then positioned on top of the previous one, under the assumption that the base coordinate frame of the new component is coaxial and coincident with the coordinate frame located at the center of the top surface of the component below it.

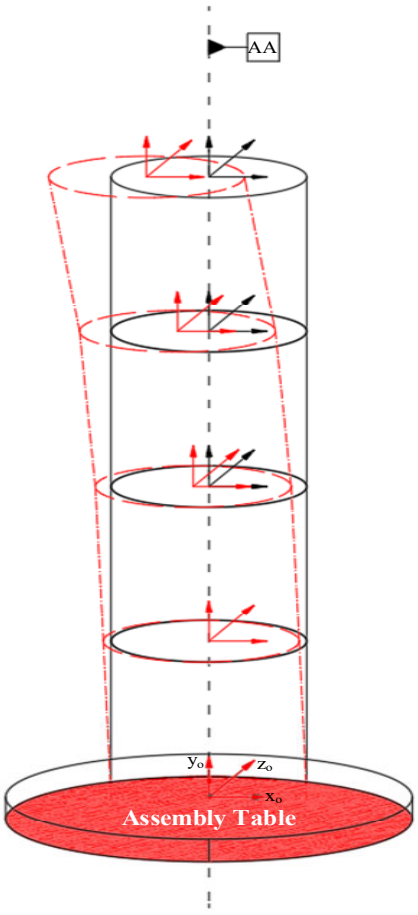

Fig. 5. Assembly of nominal and actual axisymmetric cylindrical components.

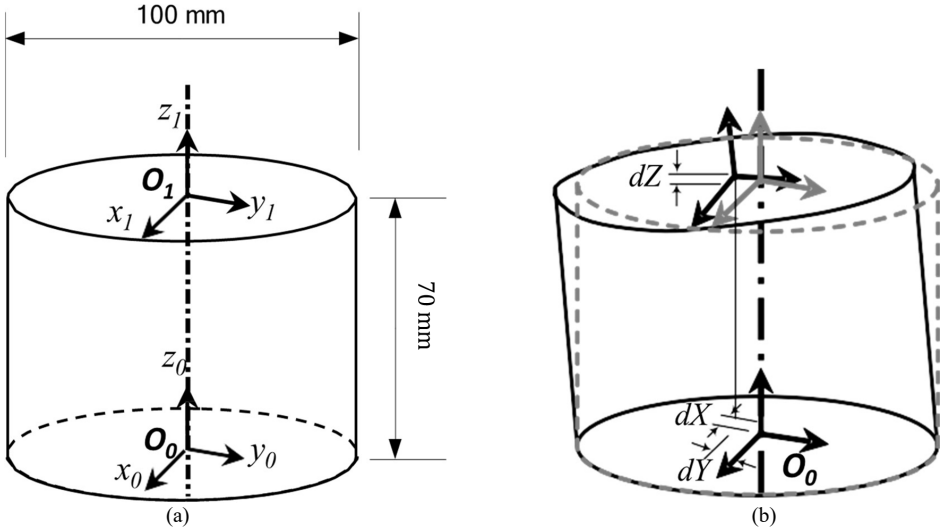

Fig. 6. A cylindrical component: (a) nominal geometry; (b) deviation from nominal dimensions [22].

TABLE II. DIMENSIONS AND ASSUMPTIONS FOR CYLINDRICAL COMPONENTS

Parameters	Value
Number of components	4
Nominal height of each component	70 mm
Nominal diameter	100 mm
Translation errors $(d\theta_{xi}, d\theta_{yi}, d\theta_{zi})$	0.1 mm
Size tolerance $(\pm T_s)$	±0.1 mm

However, due to geometric imperfections in the manufactured components, as shown in Fig. 6(b), the final assembled structure deviates from its nominal vertical alignment. For analysis, uniform translational errors (dx_i, dy_i, dz_i) are assumed for each component. A key geometric characteristic used to evaluate deviation is the eccentricity error, defined as the perpendicular offset between the central axis of the component and the global datum axis (AA), and can be calculated as shown in Eq. (26).

$$Eccentricity = \sqrt{(dp_i^X)^2 + (dp_i^Y)^2} \quad (26)$$

The terms, dp_i^X, and dp_i^Y, in Eq. (26), represent the errors along the x, and y axes, respectively, and are computed using Eq. (20). The rotation matrix R_i is considered to be the identity matrix, while the translation vector p_i is defined as $[0,0,70]^T$.

The analysis considers the worst-case assembly of components, where each component's translational and rotational error is assumed to reach its maximum limit. The performance of the developed model is evaluated across a range of angular orientation errors (in degrees) as defined by Eq. (27) for assemblies comprising 4, 6, and 8 components.

Moreover, to assess the impact of geometric variations on assembly variation propagation, the model performance is also evaluated across a set of geometric run-out tolerances in mm as defined in Eq. (28), using defined geometric tolerances, axial run-out (T_{ar}) and radial run-out (T_{rr}) and size tolerance $(\pm T_s)$ for each assembly configuration.

$$d\theta_{xi} = d\theta_{yi} = d\theta_{zi} = \begin{bmatrix} 0.001,0.005,0.01,0.05,0.10,0.15,0.20,0.25,0.30,0.35,0.40, \\ 0.45,0.50,0.55,0.60,0.65,0.70,0.75,0.80,0.85,0.90,0.95,1.0 \end{bmatrix} \text{deg} \quad (27)$$

$$T_{ar} = T_{rr} = \begin{bmatrix} 0.001,0.005,0.01,0.05,0.10,0.15,0.20,0.25,0.30,0.35,0.40,0.45, \\ 0.50,0.55,0.60,0.65,0.70,0.75,0.80,0.85,0.90,0.95,1.0 \end{bmatrix} mm \quad (28)$$

Monte Carlo Simulation (MCS) is a widely adopted numerical method for analyzing the statistical behavior of assemblies influenced by random geometric variations [25]. It is a standard approach in tolerance analysis and is based on generating random samples of component tolerances [26]. In this study, MCS is employed to simulate the assembly process by sequentially joining the mating features of individual components. Manufacturing variations are modeled as zero-mean Gaussian random variables, with the standard deviation (σ) is taken as one-third of the specified tolerance. The results are calculated for assembly errors $(dp_i^X, dp_i^Y, dp_i^Z,)$ and the corresponding eccentricity of the final assembly.

The study investigates run-out tolerances (T_{ar}) and (T_{rr}) at three distinct values of 0.01, 0.1, and 1 mm, while taking the size tolerance $(\pm T_s)$ fixed at 0.1 mm. The simulation generates 10,000 random assembly iterations within these tolerance bounds.

IV. VALIDATION OF THE DEVELOPED MODEL

The effectiveness of the proposed model is validated by comparing its performance with two established approaches described in Ref. [22]: the linear connective assembly model and the fully nonlinear connective assembly model. The linear model simplifies geometric relationships using a first-order approximation, allowing it for efficient execution time but with reduced accuracy in predicting geometric deviations. In contrast, the fully nonlinear connective assembly model incorporates full trigonometric expansions to account for higher-order deviations, offering high predictive accuracy at the expense of computational cost.

The proposed model retains second-order nonlinear terms in the homogeneous transformation matrices, offering improved accuracy over the linear model while maintaining significantly lower computational complexity than the fully nonlinear model. For a robust comparative evaluation, numerical analyses have been conducted for assemblies consisting of 4, 6, and 8 axisymmetric cylindrical components. The evaluation is based on two principal criteria: (1) angular orientation errors, (2) geometric runout tolerances, and the results are presented in Figs. 7–12.

In order to further validate these findings, Monte Carlo simulations, conducted within a defined dimensional tolerance zone of $(\pm T_s)$ = 0.1 mm. The run-out tolerances at 0.01 mm, 0.1 mm and 1.0 mm were selected to represent high, moderate, and low assembly precision levels, thereby covering the practical spectrum of deviations encountered in high-precision assemblies. The size tolerance $(\pm Ts)$ was held fixed at 0.1 mm, as industrial practice generally maintains size tolerance as fixed to isolate the influence of run-out on variation propagation. This ensures that the observed differences in predictive performance are directly linked to runout effects.

This setup enables a statistically robust assessment of the proposed model's sensitivity and reliability under varying runout tolerances [22]. This approach is consistent

with GD&T practice, where run-out tolerance is specified independently of size tolerance based on functional and rotational requirements [27]. The results presented in Fig. 13–15 illustrate the improved predictive accuracy of the proposed model.

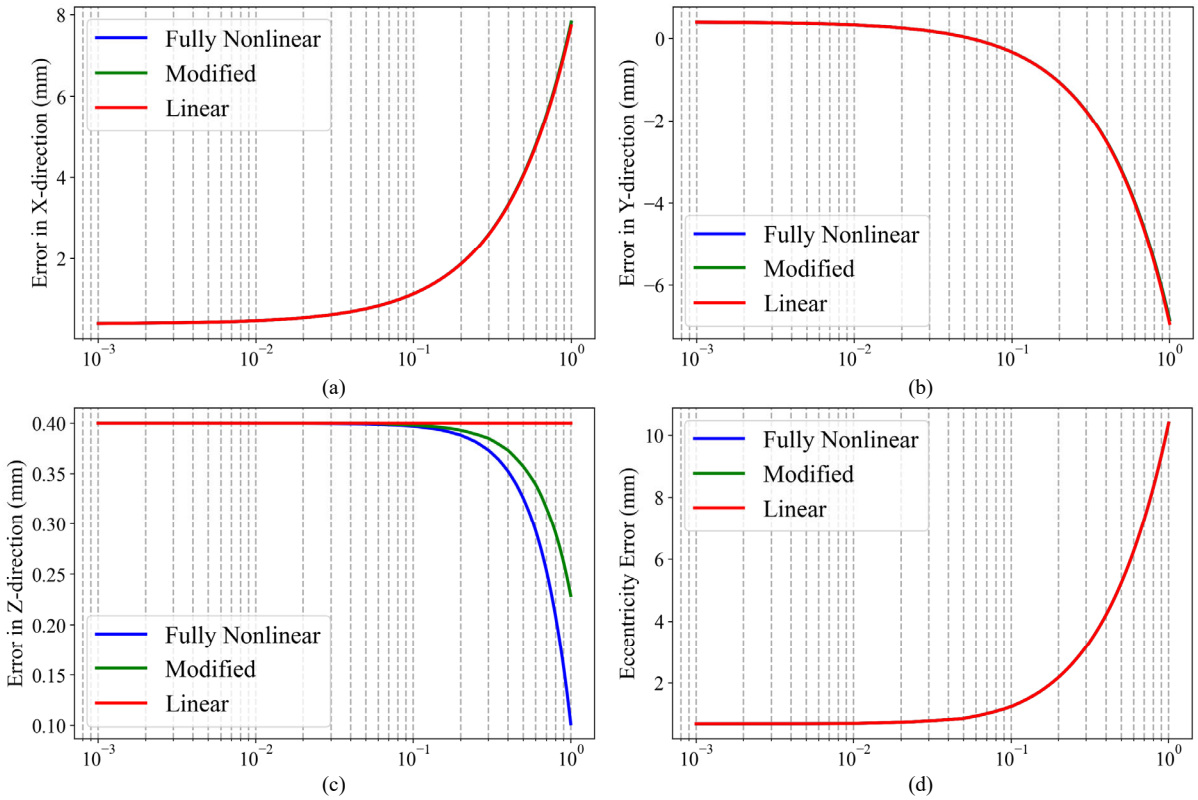

Fig. 7. Comparison of final-stage assembly variations across a range of angular orientation errors: (a) errors in X-direction, (b) errors in Y-direction, (c) errors in Z-direction, and (d) eccentricity errors for 4 components.

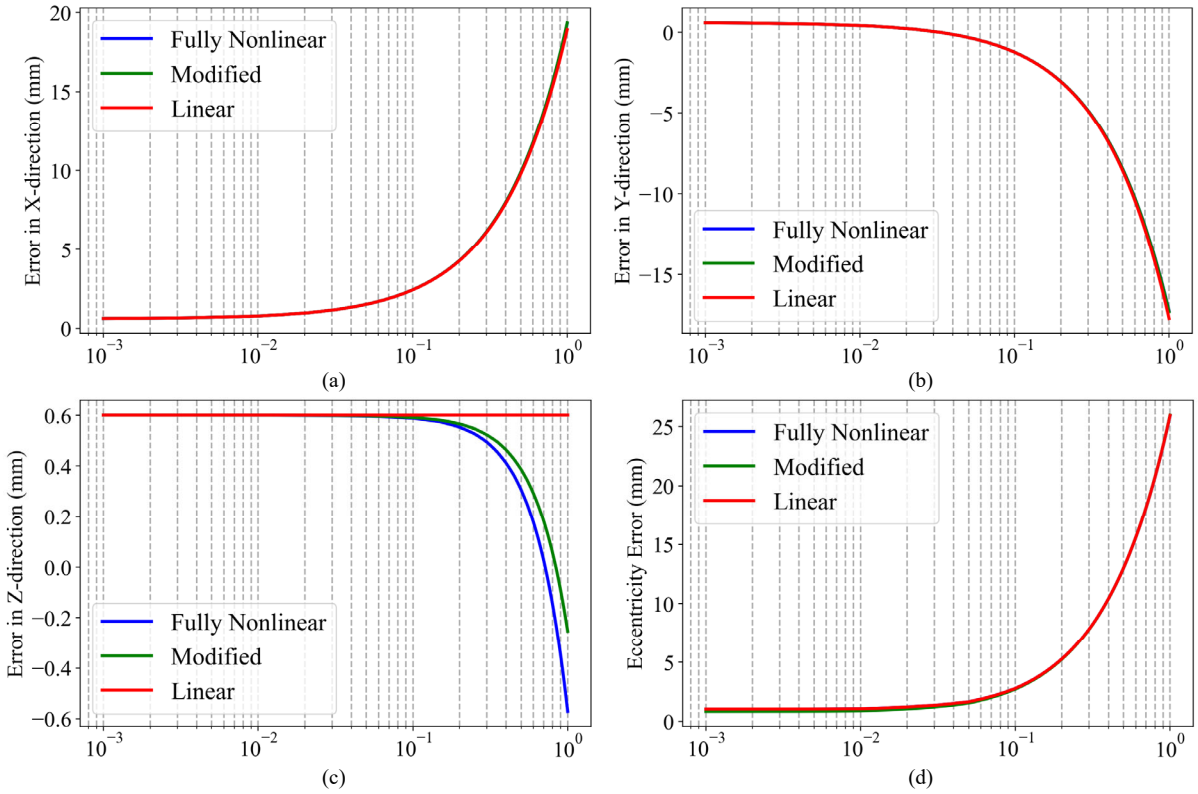

Fig. 8. Comparison of final-stage assembly variations across a range of angular orientation errors: (a) errors in X-direction, (b) errors in Y-direction, (c) errors in Z-direction, and (d) eccentricity errors for 6 components.

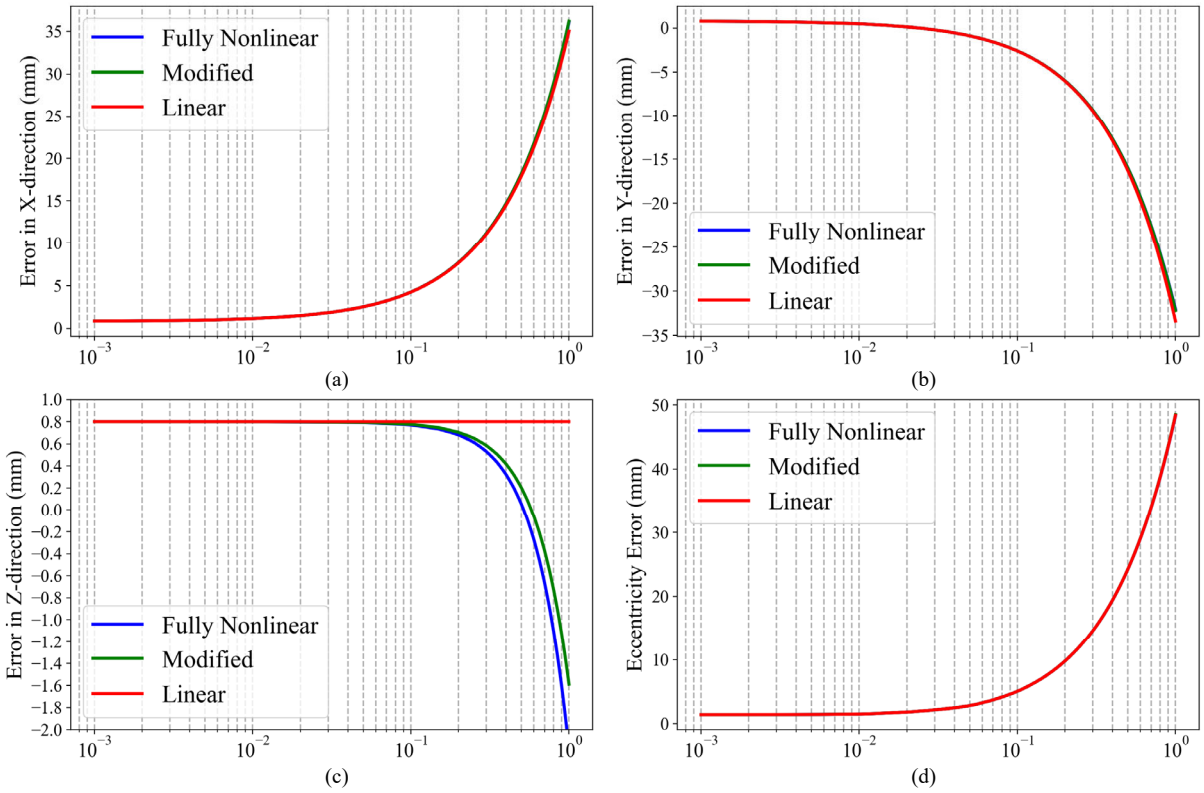

Fig. 9. Comparison of final-stage assembly variations across a range of angular orientation errors: (a) errors in X-direction, (b) errors in Y-direction, (c) errors in Z-direction, and (d) eccentricity errors for 8 components.

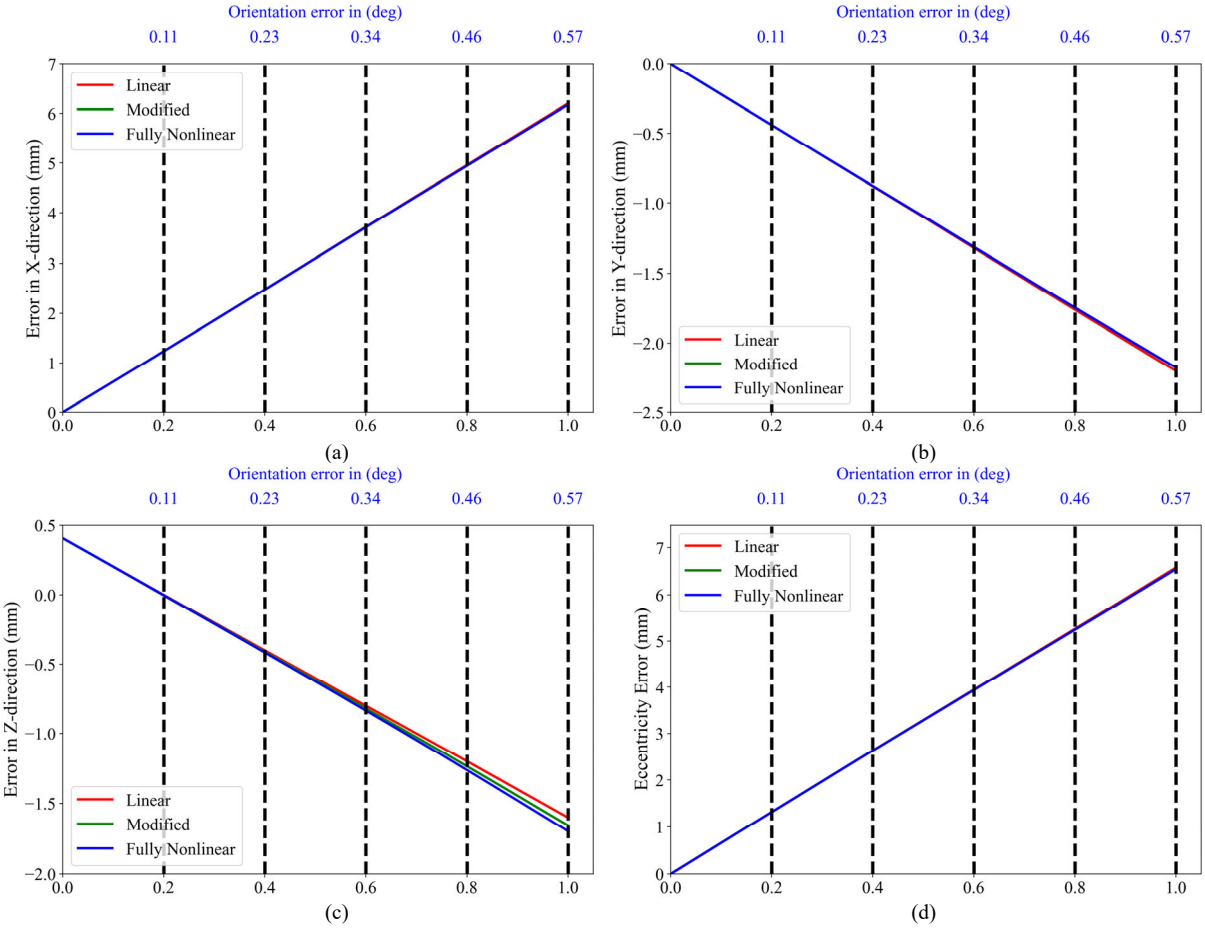

Fig. 10. Comparison of final-stage assembly variations across a range of geometric runout tolerances: (a) errors in X-direction, (b) errors in Y-direction, (c) errors in Z-direction, and (d) eccentricity errors for 4 components.

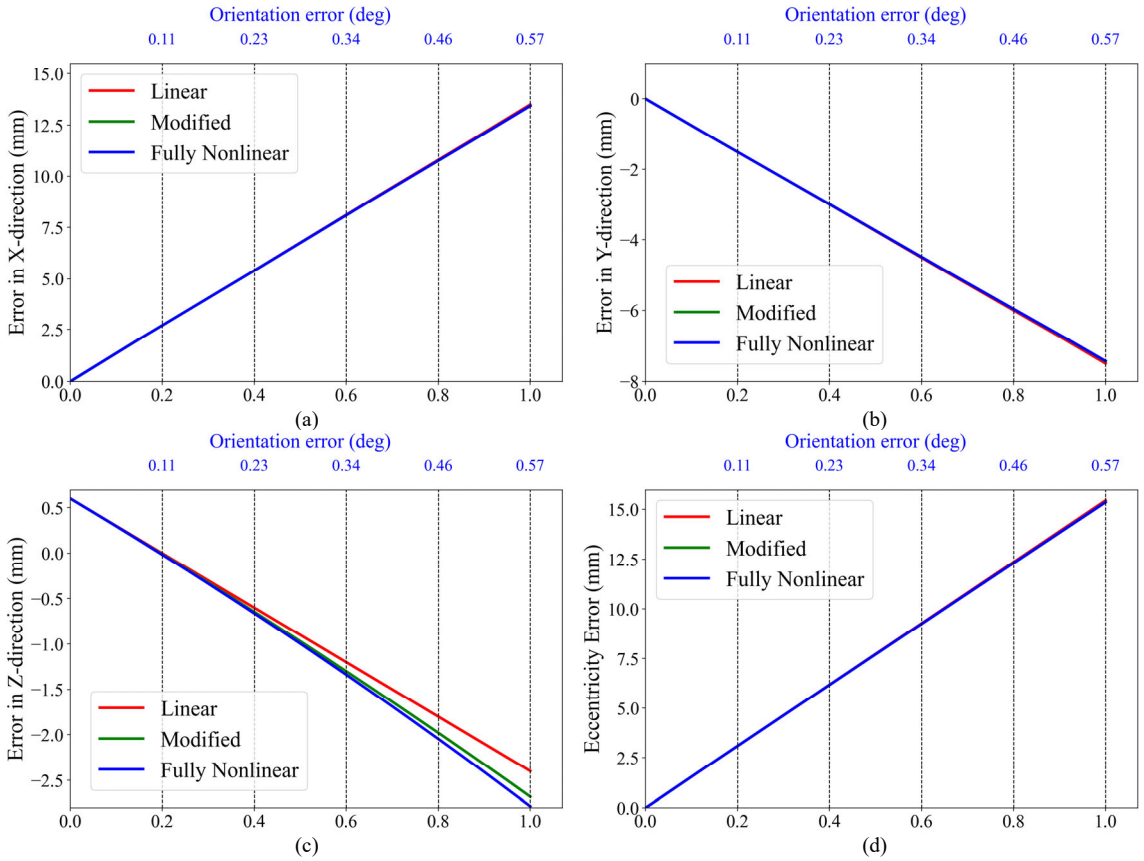

Fig. 11. Comparison of final-stage assembly variations across a range of geometric runout tolerances: (a) errors in X-direction, (b) errors in Y-direction, (c) errors in Z-direction, and (d) eccentricity errors for 6 components.

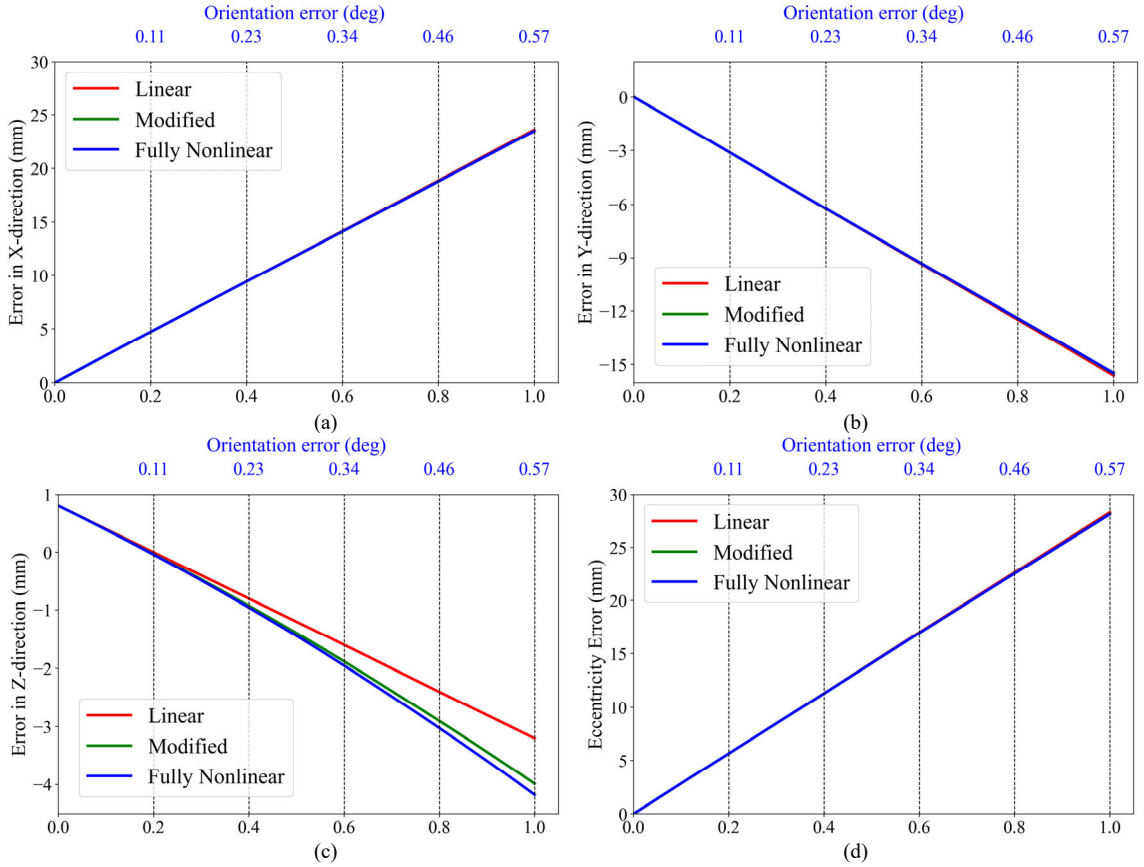

Fig. 12. Comparison of final-stage assembly variations across a range of geometric runout tolerances: (a) errors in X-direction, (b) errors in Y-direction, (c) errors in Z-direction, and (d) eccentricity errors for 8 components.

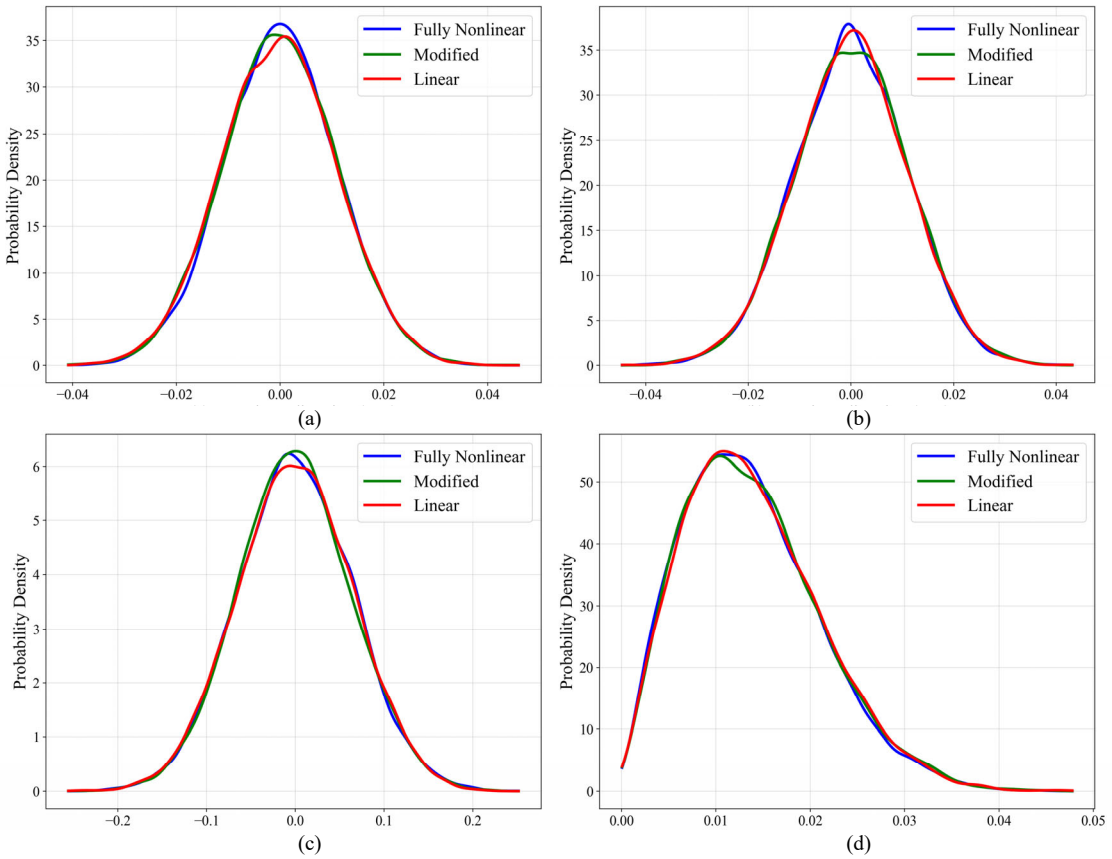

Fig. 13. Probability density functions of final assembly errors: (a) errors in X-direction, (b) errors in Y-direction, (c) errors in Z-direction, and (d) eccentricity errors for 4 components at axial and radial runout tolerance of 0.01 mm.

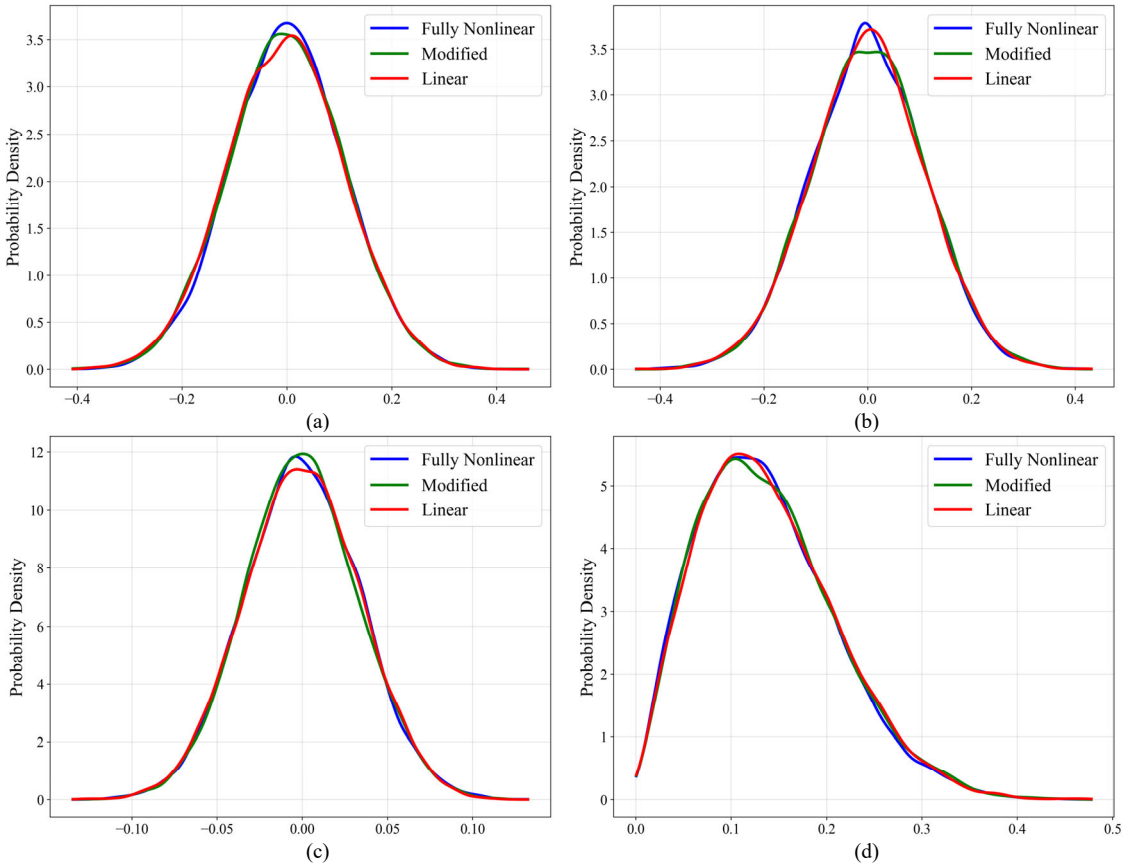

Fig. 14. Probability density functions of final assembly errors: (a) errors in X-direction, (b) errors in Y-direction, (c) errors in Z-direction, and (d) eccentricity errors for 4 components at axial and radial runout tolerance of 0.1 mm.

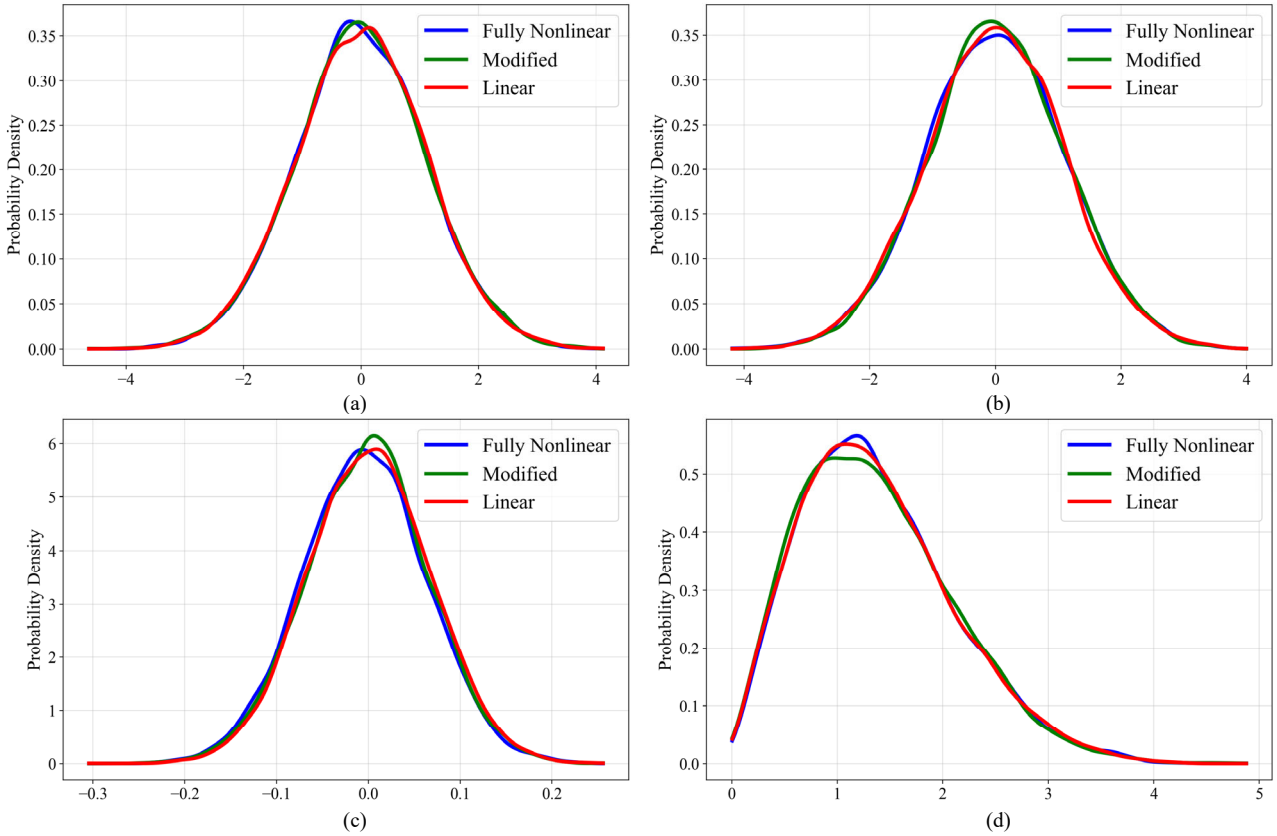

Fig. 15. Probability density functions of final assembly errors: (a) errors in X-direction, (b) errors in Y-direction, (c) errors in Z-direction, and (d) eccentricity errors for 4 components at axial and radial runout tolerance of 1.0 mm.

V. Result and Discussion

Accurate prediction of geometric errors in high-precision assemblies is essential to maintain dimensional accuracy and functional performance, and manufacturing reliability. The performance of the proposed assembly model was evaluated by comparing it with the existing linear and the fully nonlinear models for assemblies composed of 4, 6, and 8 axisymmetric cylindrical components. The comparative analysis focused on angular orientation errors, geometric run-out tolerances, and MCS results. As illustrated in Figs. 7–9, the variation in positional errors (dp_x, dp_y, dp_z) and eccentricity under increasing angular orientation errors ranging from 0.001° to 1.0° highlights the effectiveness of the modified model.

Across all three assembly models, the proposed model shows strong agreement with both reference models for errors (dp_x, dp_y) and eccentricity, indicating that the proposed model can accurately predict radial and axial deviations across a wide range of angular orientation errors. More significant differences are evidenced in the Z-direction error (dp_z). At small orientation errors (<0.1°), all three models exhibit similar behavior. However, at 1.0°, their discrepancies are clear. For the assembly of 4 components, the linear model predicts a Z-error of 0.40 mm, while the modified model predicts 0.23 mm, closer to the 0.10 mm obtained from the fully nonlinear model. For the assembly of 6 components, the linear model predicts 0.60 mm, compared to −0.25 mm from the modified model, and −0.57 mm from the fully nonlinear model. The divergence is more significant in the assembly of 8 components, where the linear model predicts 0.80 mm, while the modified model predicts −1.59 mm, closely aligning with −2.18 mm predicted by the fully nonlinear model. The comparison of results are further illustrated in Table III, which shows that the modified model reduces the Z-direction error by 56.67%, 72.65%, and 80.20% for assemblies of 4, 6, and 8 components, respectively, thereby confirming its capability to predict the nonlinear assembly behavior more effectively than the linear model.

TABLE III. Comparison of Z-Direction Errors at 1° Angular Orientation

No. of Components	Models	Z-Error (mm)	Improvement vs. Linear Model (%)
4	Linear	0.40	-
	Modified	0.23	56.67
	Fully nonlinear	0.10	-
6	Linear	0.60	-
	Modified	−0.25	72.65
	Fully nonlinear	−0.57	-
8	Linear	0.80	-
	Modified	−1.59	80.20
	Fully nonlinear	−2.18	-

A Similar trend was also observed in Figs. 10–12, which illustrates the influence of geometric runout tolerances on assembly errors for stacks of 4, 6, and 8 cylindrical components. The modified model remains in close agreement with both the linear and fully nonlinear models for errors (dp_x, dp_y) and eccentricity. The Z-direction error (dp_z) once again highlights the distinction between the models. At small runout tolerances (<0.2 mm), all three models predict nearly identical results. As the tolerance increases, the linear model diverges, underestimating the nonlinear error response. In contrast, the modified model continues to follow the fully nonlinear trend more closely, particularly as the tolerance approaches 1.00 mm.

For the assembly of 4 components, the linear model predicts a Z-error of −1.60 mm, the modified model predicts −1.66 mm**,** and the fully nonlinear model predicts −1.70 mm. In the assembly of 6 components, the linear model predicts −2.40 mm, compared to −2.68 mm from the modified model and −2.79 mm from the fully nonlinear model. This discrepancy becomes more significant for the assembly of 8 components, where the linear model predicts −3.20 mm, whereas the modified model predicts −3.99 mm, which is close to the −4.18 mm obtained from the fully nonlinear model. As summarized in Table IV, the modified model improves prediction accuracy relative to the linear model by approximately 60.00% for 4 components, 71.79% for 6 components, and 80.61% for 8 components, respectively confirming its robustness in modeling nonlinear effects under increasing geometric runout tolerances.

TABLE IV. COMPARISON OF Z-DIRECTION ERRORS AT 1 MM RUNOUT TOLERANCE

No. of Components	Models	Z-Error (mm)	Improvement vs. Linear Model (%)
4	Linear	−1.60	-
	Modified	−1.66	60.00
	Fully nonlinear	−1.70	-
6	Linear	−2.40	-
	Modified	−2.68	71.79
	Fully nonlinear	−2.79	-
8	Linear	−3.20	-
	Modified	−3.99	80.61
	Fully nonlinear	−4.18	-

TABLE V. COMPARISON OF MODELS FOR EXECUTION TIME

Models	Execution Time (s)	Time Reduction
Linear	2.53	-
Modified	4.82	48.39%
Fully nonlinear	9.34	Baseline Model

Further validation of the modified model was carried out using MCS for the 4 components assembly only, as illustrated in Figs. 13–15. The statistical analysis confirms that the modified model closely follows the results of the fully nonlinear model. The positional errors follow zero-mean Gaussian distributions, while the eccentricity follows a Rayleigh distribution. When increasing the geometric runout tolerance from 0.01 mm to 1.0 mm results in a proportional increase in the magnitude of positional errors and eccentricity, while the general shape of the distribution remains relatively unchanged.

This behavior shows that tolerance amplification affects error magnitude but does not alter the underlying statistical nature of deviations. In terms of computational efficiency, the modified model shows a considerable advantage. As shown in Table V, the linear model provides the shortest execution time of 2.53 s, but its predictions lack accuracy. The fully nonlinear model delivers the most accurate results but requires 9.34 s, making it computationally intensive. By contrast, the modified model achieves nearly the same accuracy as the fully nonlinear model but with a reduced execution time of 4.82 s, representing a 48.39% improvement in computational efficiency. The reduction in computational time is achieved not through algorithmic shortcuts, but by retaining only second-order terms in the matrix multiplications to avoid the higher-order trigonometric expansions inherent to the fully non-linear model. This enables the modified model to achieve an effective balance between prediction accuracy and execution time.

In existing literature, the comparison between linear and fully non-linear models has predominantly been undertaken through MCS, owing to the inherent complexity of the fully non-linear model, which precludes direct analysis via conventional numerical methods. Conversely, for the linear model, an independent numerical framework was developed and validated separately. In the present study, MCS serves as the sole approach for uncertainty quantification and validation of the second-order assembly variation propagation model. To strengthen the robustness and generalizability of the findings, future research will aim to integrate advanced probabilistic methodologies to facilitate more comprehensive comparative analyses and enhance the computational efficiency of uncertainty propagation.

VI. CONCLUSION

This study presented the development and validation of a modified connective assembly model for predicting geometric errors in high-precision multi-stage assemblies of axisymmetric cylindrical components. The model was compared with the linear model and the fully nonlinear model under angular orientation errors, geometric runout tolerances, and MCS. The findings show that while the linear model provides acceptable predictions only at very small deviations, it fails to predict nonlinear effects at larger angular or geometric tolerances. In contrast, the modified model shows strong agreement with the fully nonlinear model across all investigated cases. For angular orientation errors at 1.0°, the modified model achieved predictive accuracy of 56.67% for 4-component assembly, 72.65% for 6 components, and 80.20% for 8 components when compared with the linear model. Similarly, for geometric runout tolerances at 1.0 mm, the modified model improved accuracy by 60.00% for

4 components, 71.79% for 6 components, and 80.61% for 8 components relative to the linear model. Monte Carlo simulations, performed on the 4-component assembly across tolerance ranges from 0.01 mm to 1.0 mm, further validated the effectiveness of the modified model. The results confirmed that positional errors (dp_x, dp_y, dp_z) follow zero-mean Gaussian distributions, while eccentricity follows a Rayleigh distribution, consistent with the fully nonlinear model. Furthermore, the modified model achieved these results with a significantly reduced computational cost, requiring only 4.82 s compared to 9.344 s for the fully nonlinear model, representing 48.39% improvement in computational efficiency.

CONFLICT OF INTEREST

The authors declare no conflict of interest.

AUTHOR CONTRIBUTIONS

MA conceptualized the modified connective assembly model, derived mathematical formulations, performed simulations, analyzed error propagation, and wrote the original draft; TH critically supervised the nonlinear error propagation modeling and technically reviewed the manuscript; NHM contributed to methodology improvement and helped in manuscript drafting; AAS contributed to model development and validated the results against existing models; all authors had approved the final version.

FUNDING

This work was supported by the Higher Education Commission (HEC) of Pakistan under the "Aghaz-e-Haqooq-Balochistan Package" (Project SAP Nos: 1500022297/23484, 1500029055/272, 1500004230/9646, and 1500018966/91).

ACKNOWLEDGMENT

The authors also gratefully acknowledge Mehran University of Engineering & Technology, Jamshoro, Sindh, Pakistan, for providing the research facilities and platform essential to this study.

REFERENCES

[1] Z. Li and X. Zheng, "Review of design optimization methods for turbomachinery aerodynamics," *Progress in Aerospace Sciences*, vol. 93, pp. 1–23. doi: 10.1016/j.paerosci.2017.05.003

[2] R. Mantripragada and D. E. Whitney, "Modeling and controlling variation propagation in mechanical assemblies using state transition models," *IEEE Transactions on Robotics and Automation*, vol. 15, no. 1, pp. 124–140, 2002. doi: 10.1109/70.744608

[3] S. Shi, J. Liu, H. Gong *et al.,* "Assembly accuracy analysis and phase optimization of aero-engine multistage rotors considering surface morphology and non-uniform contact deformation," *Precis Eng.*, vol. 88, pp. 595–610, 2024. doi: 10.1016/j.precisioneng.2024.04.003

[4] Y. Liu, M. Zhang, C. Sun *et al.,* "A method to minimize stage-by-stage initial unbalance in the aero engine assembly of multistage rotors," *Aerosp Sci Technol.,* vol. 85, pp. 270–276, 2019. doi: 10.1016/j.ast.2018.12.007

[5] T. Hussain, Z. Yang, A. A. Popov *et al.,* "Straight-build assembly optimization: A method to minimize stage-by-stage eccentricity error in the assembly of axisymmetric rigid components (two-dimensional case study)," *J Manuf. Sci. Eng.,* vol. 133, no. 3, 031014, 2011. doi: 10.1115/1.4004202

[6] Z. Yang, S. McWilliam, A. A. Popov *et al.,* "Dimensional variation propagation analysis in straight-build mechanical assemblies using a probabilistic approach," *J. Manuf. Syst.,* vol. 32, no. 2, pp. 348–356, 2013. doi: 10.1016/j.jmsy.2012.11.008

[7] T. Hussain, S. McWilliam, A. A. Popov *et al.,* "Geometric error reduction in the assembly of axi-symmetric rigid components: A two-dimensional case study," in *Proc. Inst. Mech. Eng. B. J. Eng. Manuf.,* vol. 226, no. 7, pp. 1259–1274, 2012. doi: 10.1177/0954405412443471

[8] L. Wang, C. Sun, J. Tan *et al.,* "Improvement of location and orientation tolerances propagation control in cylindrical components assembly using stack-build assembly technique," *Assembly Automation*, vol. 35, pp. 358–366, 2015. doi: 10.1108/AA-03-2015-023

[9] C. Z. Sun, L. Wang, J. B. Tan *et al.,* "Improvement of variation propagation control in mechanical assembly using adjustment assembly technique," *Applied Mechanics and Materials,* vol. 870, pp. 459–464, 2017. doi: 10.4028/www.scientific.net/amm.870.459

[10] Y. Zhao, X. Mu, J. Liu *et al.,* "A decoupling algorithm-based technology for predicting and regulating the unbalance of aircraft rotor assembly considering manufacturing errors," *Machines,* vol. 11, no. 10, 970, 2023. doi: 10.3390/machines11100970

[11] M. Zhang, Y. Liu, D. Wang *et al.,* "A coaxiality measurement method for the aero-engine rotor based on common datum axis," *Measurement (Lond)*, vol. 191, 110696, 2022. doi: 10.1016/j.measurement.2022.110696

[12] S. Ding, S. Jin, Z. Li *et al.,* "Multistage rotational optimization using unified Jacobian–Torsor model in aero-engine assembly," in *Proc. Inst. Mech. Eng. B. J. Eng. Manuf.,* vol. 233, no. 1, pp. 251–266, 2019. doi: 10.1177/0954405417703431

[13] S. Jin, S. Ding, Z. Li *et al.,* "Point-based solution using Jacobian-Torsor theory into partial parallel chains for revolving components assembly," *J. Manuf. Syst.,* vol. 46, pp. 46–58, 2018. doi: 10.1016/j.jmsy.2017.11.003

[14] Y. Sun, J. Guo, J. Hong *et al.,* "Repair decision based on sensitivity analysis for aero-engine assembly," *International Journal of Precision Engineering and Manufacturing*, vol. 20, pp. 347–362, 2019. doi: 10.1007/s12541-019-00094-0

[15] M. Li, Y. Wang, Q. Sun *et al.,* "Assembly accuracy prediction and optimization of aero-engine rotor under the separation condition of assembly and measurement," *International Journal of Advanced Manufacturing Technology*, vol. 120, pp. 3103–3112, 2022. doi: 10.1007/s00170-022-08912-y

[16] X. Zhang, X. Fu, B. Fu *et al.,* "Multi-objective optimization of aeroengine rotor assembly based on tensor coordinate transformation and NSGA-II," *CIRP J Manuf Sci Technol*, vol. 51, pp. 190–200, 2024. doi: 10.1016/j.cirpj.2024.04.004

[17] T. Zhou and H. Gao, "Modeling and simulation of the assembly accuracy of aero-engine rotors in the docking processes using a specially designed novel multi-DOF NC motion platform," *Aerosp Sci. Technol.*, vol. 113, 106648, 2021. doi: 10.1016/j.ast.2021.106648

[18] T. Zhou, H. Gao, X. Wang *et al.,* "Error modeling and compensating of a novel 6-DOF aeroengine rotor docking equipment," *Chinese Journal of Aeronautics*, vol. 35, pp. 312–324, 2022. doi: 10.1016/j.cja.2021.04.009

[19] Y. Yi, T. Liu, Y. Yan *et al.,* "A novel assembly tolerance analysis method considering form errors and partial parallel connections," *International Journal of Advanced Manufacturing Technology*, vol. 131, no. 11, pp. 5489–5510, 2024. doi: 10.1007/s00170-022-09628-9

[20] Y. Zhang, Q. Zhang, Y. Hu *et al.,* "A surrogate modeling framework for aircraft assembly deformation using triplet attention-enhanced conditional autoencoder," *J. Manuf. Syst.,* vol. 77, pp. 708–729, 2024. doi: 10.1016/j.jmsy.2024.10.009

[21] Y. Liu, Y. Ren, Q. Lin *et al.,* "A digital twin-based assembly model for multi-source variation fusion on vision transformer," *J. Manuf. Syst.,* vol. 76, pp. 478–501, 2024. doi: 10.1016/j.jmsy.2024.08.011

[22] T. Hussain, "Modelling and controlling variation propagation in mechanical assembly of high speed rotating machines," PhD thesis, Dept. of Mechan. Mater. and Manufacturing Eng., Univ. of Nottingham, 2012.

[23] D. E. Whitney, *Mechanical Assemblies: Their Design, Manufacture, and Role in Product Development*, New York: Oxford university press, 2004.
[24] G. Henzold, *Geometrical Dimensioning and Tolerancing for Design, Manufacturing and Inspection: A Handbook for Geometrical Product Specification using ISO and ASME Standards*, Elsevier, 2006.
[25] M. L. Stewart and K. W. Chase, "Variation simulation of fixtured assembly for compliant structures using piecewise-linear analysis," in *Proc. American Society of Mechanical Engineers, Manufacturing Engineering Division (MED)*, 2005, pp. 591–600. doi: 10.1115/IMECE2005-82371
[26] C. G. Glancy and K. W. Chase, "A second-order method for assembly tolerance analysis," in *Proc. the ASME Design Engineering Technical Conf.,* 1999, pp. 977–984. doi: 10.1115/DETC99/DAC-8707
[27] S. Tornincasa, "Run-out tolerances," in *Technical Drawing for Product Design*, Springer Tracts in Mechanical Engineering. Springer, Cham, 2024, pp. 311–327. doi: 10.1007/978-3-031-51187-5_11